



Real-time measurement of phase partitioning of organic compounds using a proton-transfer-reaction time-of-flight mass spectrometer coupled to a CHARON inlet

Yarong Peng^{1,2}, Hongli Wang², Yaqin Gao², Shengao Jing², Shuhui Zhu², Dandan Huang², Peizhi Hao³, Shengrong Lou², Tiantao Cheng^{4,5}, Cheng Huang², and Xuan Zhang³

¹Department of Environmental Science and Engineering, Fudan University, Shanghai, 200438, China

²State Environmental Protection Key Laboratory of Formation and Prevention of Urban Air Pollution Complex, Shanghai Academy of Environmental Sciences, Shanghai, 200233, China

³School of Natural Sciences, University of California, Merced, 95343, USA

⁴Department of Atmospheric and Oceanic Sciences, Fudan University, Shanghai, 200438, China

⁵Big Data Institute for Carbon Emission and Environmental Pollution, Fudan University, Shanghai, 200438, China

Correspondence: Hongli Wang (wanghl@saes.sh.cn), Tiantao Cheng (ttcheng@fudan.edu.cn) and Xuan Zhang (xzhang87@ucmerced.edu)

Received: 3 May 2022 – Discussion started: 28 June 2022

Revised: 3 December 2022 – Accepted: 5 December 2022 – Published: 4 January 2023

Abstract. Understanding the gas–particle partitioning of semivolatile organic compounds (SVOCs) is of crucial importance in the accurate representation of the global budget of atmospheric organic aerosols. In this study, we quantified the gas- vs. particle-phase fractions of a large number of SVOCs in real time in an urban area of East China with the use of a CHEMICAL ANALYSIS OF aeROSOLS ON-line (CHARON) inlet coupled to a high-resolution proton-transfer-reaction time-of-flight mass spectrometer (PTR-ToF-MS). We demonstrated the use of the CHARON inlet for highly efficient collection of particulate SVOCs while maintaining the intact molecular structures of these compounds. The collected month-long dataset with hourly resolution allows us to examine the gas–particle partitioning of a variety of SVOCs under ambient conditions. By comparing the measurements with model predictions using instantaneous equilibrium partitioning theory, we found that the dissociation of large parent molecules during the PTR ionization process likely introduces large uncertainties to the measured gas- vs. particle-phase fractions of less oxidized SVOCs, and therefore, caution should be taken when linking the molecular composition to the particle volatility when interpreting the PTR-ToF-MS data. Our analysis suggests that understanding the fragmentation mechanism of SVOCs and accounting for

the neutral losses of small moieties during the molecular feature extraction from the raw PTR mass spectra could reduce, to a large extent, the uncertainties associated with the gas–particle partitioning measurement of SVOCs in the ambient atmosphere.

1 Introduction

Gas–particle partitioning of semivolatile organic compounds (SVOCs) is a critical process involved in the formation and evolution of atmospheric organic aerosols (OA). Traditionally, gas–particle equilibrium partitioning of organic substances is assumed to be established instantaneously (Zhang and Seinfeld, 2013); this assumption is in question if particles are semi-solid or glassy (Shiraiwa et al., 2013). Most studies to date addressing the kinetic limitations in partitioning have used indirect and/or theoretical methods that lack chemical and molecular specificity (Mai et al., 2015; Shiraiwa and Seinfeld, 2012). Direct measurements of gas–particle partitioning of SVOCs are needed in order to develop accurate parameterizations for the organic aerosol formation in climate models.

The major challenge in the characterization of gas–particle partitioning of SVOCs lies in the real-time measurement of labile compounds while maintaining their intact molecular structures with minimal fragmentation (Zhang et al., 2016a, b, 2019). In recent years, soft ionization techniques coupled to mass spectrometry have been widely used for the measurement of gas-phase SVOCs at the molecular level (Veres et al., 2008; Crouse et al., 2006; Heald and Kroll, 2020). Combined with thermal desorption methods, these techniques have also been deployed to measure organic compounds in both gas and particle phases nearly simultaneously (Krechmer et al., 2016). A notable example would be the use of the Filter Inlet for Gases and AEROSols coupled with a chemical-ionization mass spectrometer (FIGAERO-CIMS) to quantify the gas–particle partitioning of a broad range of organic compounds in real time (Lopez-Hilfiker et al., 2014; Ye et al., 2021; Voliotis et al., 2021; Wang et al., 2020a; Lutz et al., 2019; Lee et al., 2018; Le Breton et al., 2018; Stark et al., 2017; Lopez-Hilfiker et al., 2016, 2015; Palm et al., 2020). A number of studies among those have reached a consensus that the thermogram method, i.e., using the calibrated thermal desorption profiles vs. temperature to derive the volatility, likely provides the best estimates of the actual phase distribution. In contrast, using the directly measured gas- and particle-phase fractions of a given analyte will most likely introduce a significant positive or negative bias to the volatility estimation due to the thermal decomposition of labile organic compounds during the desorption process (Lopez-Hilfiker et al., 2015; Stark et al., 2017). Such thermal decomposition (or ion fragmentation) artifacts, either positive or negative depending on the molecular size, have been suggested to constitute the largest uncertainties in the estimation of phase partitioning behaviors of SVOCs using the thermal desorption method at ambient pressure (Thompson et al., 2016).

Along with the line of thermal desorption method development, an inlet designed for the CHEMical Analysis of aeROSols ONline (CHARON) has been developed and coupled to a proton-transfer-reaction time-of-flight mass spectrometer (PTR-ToF-MS) in recent years. As CHARON-PTR-ToF-MS does not rely on any form of pre-concentration on surfaces, it could provide online and direct measurements of organic compounds in both phases, compared with traditional thermal desorption instruments which still need to address artifacts during the particle collection and desorption processes. Another potential advantage of CHARON-PTR-ToF-MS is that the chemical information of the collected particles can be studied qualitatively and quantitatively over a chemical composition level, even at sub-nanogram mass concentrations per molecule, owing to the well-studied ion–molecule reaction chemistry in PTR-ToF-MS (Piel et al., 2019). CHARON has shown promising potential in the real-time analysis of the chemical composition and spatiotemporal distributions of aerosols with laboratory-, ground-, and aircraft-based platforms (Piel et al., 2019; Tan et al., 2018;

Gkatzelis et al., 2018a, b; Muller et al., 2017; Eichler et al., 2017, 2015; Antonsen et al., 2017; Leglise et al., 2019; Piel et al., 2021). As a relatively new technique, the use of CHARON-PTR-ToF-MS to investigate the gas–particle partitioning of organic compounds is still quite limited. Only one study by Gkatzelis et al. (2018b) deployed CHARON, together with two other aerosol sampling inlets, to measure the OA formation and aging from monoterpenes and real plant emissions in chamber experiments. Whether the CHARON inlet can be applied to the study of gas–particle partitioning of organic compounds under the actual atmospheric conditions remains to be validated.

In this study, we assess the applicability of the CHARON inlet to the time-resolved collection of organic compounds in their native molecular state using laboratory tests with a series of authentic standards. We further employ the CHARON inlet coupled to a high-resolution PTR-ToF-MS instrument to measure an array of gaseous and particulate SVOCs in an urban area of East China. The obtained month-long hourly dataset allows us to examine the gas–particle partitioning of SVOCs spanning a range of volatilities. By comparing the measurements with model predictions using instantaneous equilibrium partitioning theory, we found that fragmentation during the PTR ionization process may introduce large uncertainties to the measured gas- vs. particle-phase fractions of less oxidized SVOCs. Understanding the dissociation patterns of parent molecules and accounting for the fragmentation losses when extracting the molecular features from the raw PTR mass spectra are needed to improve the measured accuracy of SVOC partitioning between the gas and particle phase.

2 Material and methods

2.1 Sampling site

The sampling site located in the campus of the Shanghai Academy of Environmental Science (SAES) is representative of a typical urban setting surrounded by restaurants, shopping malls, and residential and commercial buildings (Fig. S1 in the Supplement). Two traffic-heavy streets in the area (Caobao Road and Humin Highway) are located ~ 150 and 450 m lateral distance to the east of the sampling site. A few petrochemical and chemical industrial facilities are located ~ 50 km to the south and southwest of the observation site, which likely bring certain long-lived pollutants to the site at a typical wind speed of $\sim 1\text{--}3$ m s⁻¹. Major pollution sources in the area include traffic, commercial and residential activities, and regional transport (Huang et al., 2021; Peng et al., 2023). The sampling inlet of the PTR-ToF-MS instrument was installed on the roof of an eight-story building ~ 24 m above the ground. A comprehensive measurement of gas- and particle-phase compounds in the ambient air was performed from 24 October to 22 November. Dur-

ing the sampling period, the average temperature, relative humidity, and wind speed were 18.0 ± 3.0 °C, $61.0\% \pm 15.0\%$, and 1.8 ± 0.7 m s⁻¹, respectively. The prevailing wind direction in this region was from the northwest and north during the polluted period (Fig. S2).

2.2 CHARON-PTR-ToF-MS

2.2.1 Operation protocols

A proton-transfer-reaction time-of-flight mass spectrometer (PTR-ToF-MS) coupled to a Chemical Analysis of aeRosols ONline (CHARON; Ionicon Analytik Inc, Innsbruck, Austria) inlet was employed to measure the gas- and particle-phase concentrations of a series of SVOCs. The PTR-ToF-MS instrument used here is equipped with a radio-frequency-only (RF-only) quadrupole ion guide that transmits ions more efficiently (PTR-QiTOF, Ionicon Analytik Inc) but results in a low-mass cutoff (Fig. S4). The operating parameters of the PTR-ToF-MS were held constant during the entire measurement period. The drift tube pressure, temperature, and voltage were 2.9 mbar, 120 °C, and 500 V, respectively. These conditions correspond to an E/N (E is the electric field, and N is the number density of the gas molecules in the drift tube) value of ~ 100 Td ($1 \text{ Td} = 10^{-17} \text{ V cm}^2$) and a reaction time of 120 μs . Note that the E/N value determines the collision energy of ions in the reactor and therefore the degree of fragmentation and cluster formation. The operating conditions were selected for the purpose of relatively low fragmentation intensities (compared to 120–140 Td) and limited production of water clusters (compared to 60–80 Td). Low E/N enhances the degree of water clustering, which complicates the analysis of analyte ions due to a complex interplay between cluster formation ($\text{RH}^+(\text{H}_2\text{O})_n$) and proton transfer reactions (Holzinger et al., 2019). During the campaign, the sensitivity of the PTR-ToF-MS was in the range of 300–1000 ncps ppb⁻¹, and the mass resolution was maintained at ~ 5000 m Δm^{-1} . Mass spectra were collected at a time resolution of 10 s.

The CHARON inlet consists of (1) a gas-phase denuder (GPD) for stripping off gas-phase analytes; (2) an aerodynamic lens (ADL) for particle collimation which is combined with an inertial sampler for emanating the particle-enriched flow; and (3) a thermal desorption unit (TDU) for particle volatilization. The CHARON inlet functionality has been described in great detail by Eichler et al. (2015). The inlet we used here had a particle enrichment factor of ~ 15 , as discussed shortly. The vaporizer (TDU) was operated at 140 °C and ~ 8 mbar absolute pressure. This temperature was chosen to ensure all the unknowns observed in the field can be evaporated effectively while maintaining relatively intact molecular structures; see more details in Sect. 3.1. Measurements of organic compounds in the gas and particle phase were conducted using a parallel sampling system with two independent pumps, allowing for the selection of flow rates

specifically adjusted for each phase, resulting in the overall residence time of less than 2 s (Fig. S3).

2.2.2 Sampling alternation between gas and particle phase

Gas-phase compounds were measured by directly sampling the ambient air via a 2 m long perfluoroalkoxy (PFA) tube (1/4" OD) capped with a polytetrafluoroethylene (PTFE) filter (Mitex™ PTFE membrane, 5 μm pore size, 47 mm diameter) to prevent the clogging of particles in the PTR capillaries. The gas-phase inlet was independently connected to the PTR-ToF-MS instrument upstream of the drift tube via a pressure-controlled subsampling PEEK capillary (1/16" OD). Zero measurements were performed by overflowing catalytically (platinum at 370 °C) purified air through the inlet. Ambient particles were sampled through a stainless steel tube (3/8" OD) with a flow rate of ~ 3 L min⁻¹, out of which a flow of ~ 500 mL min⁻¹ was directed to the CHARON inlet. A PM_{2.5} cyclone was installed in front of the sampling line to remove coarse particles (> 2.5 μm). The particle-phase background was measured by placing a high-efficiency particulate air filter (HEPA; HEPA-CAP 7, GE Healthcare UK Limited, Buckinghamshire, UK) upstream of the CHARON inlet. Servo-motor-activated valves made of passivated stainless steel were used for switching between the two inlet configurations. During the campaign, CHARON-PTR-ToF-MS automatically switched between the gas and particle phase every 15 min. A detailed setup is given in Fig. S3 in the Supplement.

The built-in PTR-manager software (Ionicon Analytik GmbH, Innsbruck, Austria) offers the possibility to program sequences by which the instrument switches between different settings. It takes ~ 1 min for gases and particles to re-equilibrate when switching between these two modes. Data generated during this transition period (~ 2 min) were not considered. The instrument background was measured for 15 min every 5 h. The limits of detection (LoD) at 1 min resolution were in the range of 5.6 ± 2.9 ng m⁻³ for gases and 0.7 ± 0.5 ng m⁻³ for particles, respectively (Fig. S5). Concentrations of gaseous and particulate compounds shown here included the last 5 min of every gas-/particle-phase working mode, in order to minimize the interferences carried over from the previous working mode by allowing for a sufficient amount of equilibration time in the inlet (Piel et al., 2021). In order to synchronize the gas- and particle-phase data to calculate gas-particle partitioning, the average hourly data were then used for further analysis.

2.2.3 Sensitivity and calibration

Weekly calibrations were performed using a multicomponent calibration gas standard (Linde, USA) at five concentration levels from 0.5 to 10 ppb (Fig. S4a). The calibration mixture includes methanol, acetonitrile, acetaldehyde,

acrolein, acetone, isoprene, methyl vinyl ketone, methyl ethyl ketone, 2-pentanone, toluene, styrene, *p*-xylene, 1,3,5-trimethylbenzene, naphthalene, and α -pinene. Calibration standards with higher molecular weight were excluded because we only considered ion masses below 200 amu from the field measurement for the study of gas-particle partitioning; see discussions given in Sect. S1. Here the sensitivity of PTR-ToF-MS is defined as the normalized ion intensity of RH^+ (ncps) obtained at a mixing ratio of 1 ppb. For a given species (R), its sensitivity (S ; ncps ppb^{-1}) is a linear function of the rate constant of its reaction with H_3O^+ (k):

$$S = \frac{I_{\text{RH}^+} \times 10^6}{\frac{[R]}{N} \times 10^9} = k \times N \times 10^{-3} \times t \times \frac{T_{\text{RH}^+}}{T_{\text{H}_3\text{O}^+}} \times F_{\text{RH}^+} \quad (1)$$

$$\text{corrected } S = \frac{S}{\frac{T_{\text{RH}^+}}{T_{\text{H}_3\text{O}^+}} \times F_{\text{RH}^+}} = a \times k, \quad (2)$$

where the signals of H_3O^+ ($I_{\text{H}_3\text{O}^+}$) and RH^+ ions (I_{RH^+}) measured by the mass analyzer (in cps) can be related to the signals of H_3O^+ ($[\text{H}_3\text{O}^+]$) and RH^+ ($[\text{RH}^+]$) ions at the end of the drift tube, using their respective transmission efficiencies ($T_{\text{H}_3\text{O}^+}$ and T_{RH^+}) from the drift tube to the detector (De Gouw and Warneke, 2007). $[R]$ is the concentration of species R , and N is the number density of gas in the drift tube. The reaction time (t) is determined by the ion drift velocity. F_{RH^+} represents the fraction of product ions detected as RH^+ ions ($0 \leq F_{\text{RH}^+} \leq 1$). For non-fragmenting compounds, $F_{\text{RH}^+} = 1$. The measured sensitivity is further corrected by accounting for fragmentation and transmission efficiency, the value of which was derived from laboratory experiments (Fig. S4a). Uncertainties associated with the addition of the low-mass filter have been accounted for in the regression of individual transmission efficiency measurements on corresponding mass-to-charge ratios. The overall relative standard deviations were less than 15%. a is the slope of the linear regression of the corrected sensitivities on the proton-transfer-reaction rate coefficients (k), as shown in Fig. S4b. Following the method by Sekimoto et al. (2017), the linear regression result was used to determine the sensitivities of all uncalibrated species. The overall uncertainty was less than 15% for compounds with standards and around 50% for those without standards. Calculated sensitivity based on this method agrees well with measurements of authentic standards (Fig. S4c).

2.2.4 Enrichment factor

The CHARON inlet was calibrated routinely with pure ammonium nitrate particles to derive the enrichment factor as a function of the particle size following the procedures described in Eichler et al. (2015). In addition, we used a selection of authentic standards (Table S1) to test the effect of desorption temperature on the enrichment factor of labile

compounds. Previous studies with CHARON generally used a temperature of 140 °C to vaporize particles (Leglise et al., 2019; Gkatzelis et al., 2018b; Tan et al., 2018). Herein, we tested the TDU temperature ranging from 70 to 140 °C. The selected chemical standards were individually dissolved in distilled water (ethanol in the case of 2-pentadecanone and 1-pentadecanol) and nebulized by an atomizer (TSI 3076, Shoreview, MN, USA) that was pressurized with ultrapure zero air. The nebulizer outflow was diverted through two diffusion dryers to remove water vapor and an activated charcoal denuder (NovaCarb F, Mast Carbon International Ltd., Guildford, UK) to remove organic vapors. The resulting flow of polydisperse particles was then delivered into a differential mobility analyzer (DMA; TSI 3080) for particle size selection. The transmitted particles at a given size bin (300 nm for organics and 100–450 nm range for ammonium nitrate) were introduced into the CHARON-PTR-ToF-MS analyzer and a condensation particle counter (CPC; TSI 3775), respectively. Particle mass concentrations were calculated based on the CPC number distribution measurements by assuming a shape factor of 0.8 for ammonium nitrate particles and 1 for organic particles, respectively.

The particle enrichment factor (EF) of a given analyte i was calculated as the ratio of the PTR-ToF-MS-derived vs. CPC-derived mass concentrations of analyte i at a given particle size bin:

$$\text{VMR}_{(\text{PTR})i} = \frac{I_i}{S_i} \quad (3)$$

$$\text{VMR}_{(\text{CPC})i} = \rho_i \times V \times N_i \times V_m / \text{Mw}_i \quad (4)$$

$$\text{EF} = \frac{\text{VMR}_{(\text{PTR})i}}{\text{VMR}_{(\text{CPC})i}}, \quad (5)$$

where I_i is the normalized signal of species i (ncps) by PTR-ToF-MS, S_i is the sensitivity (ncps ppb^{-1}), VMR is the volume mixing ratio (ppb), ρ is the density of species i (g cm^{-3}), V is the volume of a particle sphere (m^3), N_i is the number concentration of particles measured by CPC (cm^{-3}), V_m is the molar volume of an ideal gas at 1 atm (22.4 L mol^{-1}), and Mw_i is the molecular weight (g mol^{-1}). As the calculated sensitivities of most organics in the absence of authentic standards are subject to uncertainties (15%–50%), we will herein use the multiplication of EF and S_i to evaluate the combined effect of CHARON enrichment and sensitivity on the measured concentrations of a given analyte i in the particle phase.

2.2.5 Data processing

Data were analyzed using the Tofware package (v3.2.0, Tofwerk Inc) within the Igor Pro software (v7.0, Wavemetrics). Using this package, time-dependent mass calibrations

were performed using four ions ($\text{H}_3^{18}\text{O}^+$, NO^+ , $\text{C}_6\text{H}_5\text{I}^+$, and $\text{C}_6\text{H}_5\text{I}_2^+$), where $\text{C}_6\text{H}_5\text{I}^+$ and $\text{C}_6\text{H}_5\text{I}_2^+$ were produced from the internal standard diiodobenzene. The relative mass deviation was within 6–8 ppm across the mass spectra. Considering the humidity dependence of reagent ions (H_3O^+ and $\text{H}_3\text{O}^+(\text{H}_2\text{O})$), the fitted product ion signals (RH^+) were normalized to a standard reagent ion of 10^6 cps (counts per second). Elemental composition was determined based on the accurate m/z (mass-to-charge ratio) and isotopic pattern analysis. A list of ~ 1600 ions was extracted, including both gas- and particle-phase ions. Molecular formulas including only C, H, and O atoms were assigned to the detected ions by the addition of one proton in cases where the elemental composition analysis returned multiple options. About 85 % of the signals were elementally resolved by the $\text{C}_x\text{H}_y\text{O}_z$ formula in ambient air mass spectra. A small number of nitrogen-containing compounds, such as nitroaromatics, were also identified but not included in the following analysis. Throughout of the context, we use the word “species” to refer to all compounds with assigned molecular formula, which may include multiple isomers.

2.3 Complementary measurements

In addition to CHARON-PTR-ToF-MS, a thermal desorption aerosol gas chromatograph (TAG) was also employed to measure a series of particle-phase organic species. Details of the TAG operation and data analysis protocols can be found in previous studies (He et al., 2020; Wang et al., 2020b; Zhu et al., 2021). The elemental composition and mass concentration of particles were measured by an Aerodyne high-resolution time-of-flight aerosol mass spectrometer (AMS), with details of operation and quality control protocols given by our recent study (Huang et al., 2021). Volatile organic compounds (VOCs; C_2 – C_{12}) were analyzed by a custom-built online gas chromatography system equipped with a mass spectrometer and a flame ionization detector (GC-MS/FID). The performance of this system can be found in our previous publications (Zhu et al., 2018; Wang et al., 2014). Meteorological parameters (ambient temperature, wind speed, wind direction, and relative humidity) were collected by an automatic weather station (Metone 590 series) mounted on the roof top of the campaign site.

2.4 Gas–particle partitioning measurements vs. modeling

The CHARON-PTR-ToF-MS measured gas- and particle-phase concentrations of a given species i can be used to calculate its particle-phase fraction ($F_{p,i}$).

$$P_i = \frac{I_{p,i} \times \left(\frac{m}{z} - 1\right)}{V_m \times S_i \times \text{EF}} \quad (6)$$

$$G_i = \frac{I_{g,i} \times \left(\frac{m}{z} - 1\right)}{V_m \times S_i} \quad (7)$$

$$F_{p,i} = \frac{P_i}{P_i + G_i}, \quad (8)$$

where P_i and G_i are the mass concentrations (ng m^{-3}) of species i in the particle and gas phase, respectively. $I_{p,i}$ and $I_{g,i}$ are the normalized signal (ncps) of the PTR-ToF-MS detected ion i in the particle and gas phase, respectively. V_m is taken as 22.4 L mol^{-1} . S_i is calculated or measured sensitivity (ncps ppb^{-1}); see details in Sect. 2.2.3. As structural isomers cannot be resolved in the mass spectra, the calculation here assumes that all isomers with the same molecular formula have the same chemical properties, i.e., saturation vapor pressures. Substitution of Eqs. (6) and (7) to Eq. (8) yields the final expression of the particle-phase fraction of species i ($F_{p,i}$), which is a function of the observed PTR-MS raw signals of species i in the gas and particle phase (in total ion counts), as well as the particle enrichment factor (EF) of species i .

$$F_{p,i} = \frac{I_{p,i}/\text{EF}}{I_{p,i}/\text{EF} + I_{g,i}} \quad (9)$$

Gas–particle partitioning of a given analyte i was also modeled using equilibrium partitioning theory (Pankow, 1994):

$$F_{p,i} = \frac{1}{1 + C_i^*/C_{\text{OA}}} \quad (10)$$

$$C_i^* = \frac{10^6 \text{Mw}_i \zeta_i p_i}{RT}, \quad (11)$$

where C_{OA} is the organic aerosol concentration measured by AMS ($\mu\text{g m}^{-3}$), C_i^* is the saturation mass concentration ($\mu\text{g m}^{-3}$), Mw_i is the molecular weight (g mol^{-1}), ζ is the activity coefficient (assumed as unity), p_i is the pure component liquid vapor pressure (Pa), R is the universal gas constant ($8.2 \times 10^{-5} \text{ m}^3 \text{ atm K}^{-1} \text{ mol}^{-1}$), and T is the ambient temperature (K). As detailed chemical information is lacking for all species detected by PTR-ToF-MS, here we use the expression given by Donahue et al. (2011) to approximate the value of C_i^* :

$$\log_{10} C_i^* = \left(n_{\text{C}}^0 - n_{\text{C}}^i\right) b_{\text{C}} - n_{\text{O}}^i b_{\text{O}} - 2 \frac{n_{\text{C}}^i n_{\text{O}}^i}{n_{\text{C}}^i + n_{\text{O}}^i} b_{\text{CO}}, \quad (12)$$

where $n_{\text{C}}^0 = 25$, $b_{\text{C}} = 0.475$, $b_{\text{O}} = 2.3$, and $b_{\text{CO}} = -0.3$.

2.5 Uncertainties in the measured and modeled gas–particle partitioning

The uncertainty associated with the PTR-MS measured concentrations in both gas and particle phases is less than 15 %

for compounds with chemical standards based on the optimally fitted transmission efficiency curve. For those in the absence of standards, their PTR sensitivities were calculated theoretically using Eqs. (1)–(2), and the uncertainty in the calculation mainly arises from the estimation of polarizability and dipole moment of the target molecule, which has been estimated to be within $\sim 50\%$ when only the elemental composition of that molecule is given (Sekimoto et al., 2017). It is important to note, however, that the uncertainty associated with the estimated PTR sensitivity has zero influence on the measured particle-phase fraction of any given compound because the sensitivity term is essentially canceled in the divisor function in Eq. (9). The uncertainty associated with the particle fraction of a given species i derived from the PTR-MS measurements arises predominantly from the EF term. Since the uncertainty of the measured EF depends on the uncertainty of $I_{p,i}$, we thus express the overall uncertainties of the measured gas–particle partitioning as

$$\text{Unc}(F_{p,i}) = \sqrt{\text{Unc}(\text{EF})^2 + \text{Unc}(I_{g,i})^2}. \quad (13)$$

With the calibration standards used in this study, the enrichment factor is calculated to be within 25% error ($\text{Unc}(\text{EF})$) (see detailed calculations listed in Tables S2 and S3), including the effect of wall loss inside the inlet tubing and the precision of the measurement. Huang et al. (2019) have tested the uncertainty of wall loss ($\text{Unc}(I_{g,i})$) in this PTR-MS instrument as 28%. Therefore, the overall uncertainty in the measured particle-phase fraction ($\text{Unc}(F_{p,i})$) was estimated as 38%.

The uncertainty associated with the modeled gas–particle partitioning arises primarily from the uncertainty in the estimation of the saturation mass concentration (C_i^*) based on the method developed by Donahue et al. (2011). In this method, the saturation mass concentration of species i is a nonlinear function of the numbers of carbon and oxygen atoms in that particular species; see Eq. (12). For each generic molecular formula, i.e., C_xH_y , C_xH_yO , $C_xH_yO_2$, and $C_xH_yO_4$, Donahue et al. (2011) have used a total of 25, 48, 18, and 10 chemical standards with known volatilities to validate the estimated saturation concentrations, and the estimated errors were taken as 34%, 16%, 25%, and 54%, respectively (see Table S6). As the $C_xH_yO_3$ group was not tested, we tentatively assumed the associated errors to be the same as the $C_xH_yO_4$ group. The extent to which these uncertainties may affect the difference between measurements and model results was discussed in detail in the Supplement (Fig. S10).

3 Results and discussion

3.1 Particle enrichment: effect of desorption temperature

Thermal desorption as a common procedure used in the chemical characterization of organic aerosols is often susceptible to fragmentation of nonrefractory compounds. Due to the high temperature used to evaporate particles collected, labile and large molecules are inevitably subject to fragmentation, thereby introducing large uncertainties to the measured mass and composition of the particulate organic compounds (Lopez-Hilfiker et al., 2015; Yatavelli et al., 2012; Zhao et al., 2013). Thermal decomposition of oxidized organic compounds has been observed at vaporizer temperature as low as 200 °C, the lowest temperature required to vaporize OA as reported (Stark et al., 2017). While decreasing the vaporizer temperature is necessary to maintain the intact structure of labile molecules, low temperature (e.g., 85 °C), however, might fail to completely evaporate the collected particles into vapors, resulting in an underestimation of the collected OA mass (Inomata et al., 2014). Here we performed a series of sensitivity tests to identify the optimal vaporizer temperature in the CHARON inlet for the measurements of organic compounds in the particle phase.

Prior to the temperature sensitivity test, we have validated that the particle enrichment factor, also known as collection efficiency and defined as the ratio of the particle mass concentration upstream to downstream of the aerodynamic lens, does not depend on the particle size. As shown in Fig. 1a, the measured EF value for ammonium nitrate particles, detected as NO_2^+ produced from the nitric acid vapor, remains constant as ~ 15 in the 150–450 nm particle size range. The lower values in the 100–150 nm size range can be explained by the lower particle transmission efficiency in the gas-phase denuder, e.g., 75%–80% for 100 nm particles (Eichler et al., 2015). Also, particles below 150 nm are less efficiently concentrated in the subsampling flow after the aerodynamic lens. Therefore, we used the monodisperse particles generated from selected organic standards at 300 nm for the temperature sensitivity test.

A number of chemical standards that are representative of alcohols, carbonyls, and carboxylic acids and with the vapor pressure ranging from 10^{-14} to 10^{-1} Pa at 25 °C (taken from EPA EPI Suite, 2012; see values given in Table S1) were used to generate organic aerosols, which, upon size selection at 300 nm, were directed to the CHARON inlet. Particle evaporation occurs downstream of the aerodynamic lens in the gas phase and on the tube and orifice surface to which submicron particles rapidly diffuse at ~ 8 mbar operating pressure. The thermal desorption unit was designed to ensure that ammonium sulfate particles (10^{-20} Pa) can be completely evaporated (Piel et al., 2019; Eichler et al., 2015). As the desorption temperature was varied from 70 to 140 °C, the intensities of all detected ions (including both parent and fragment

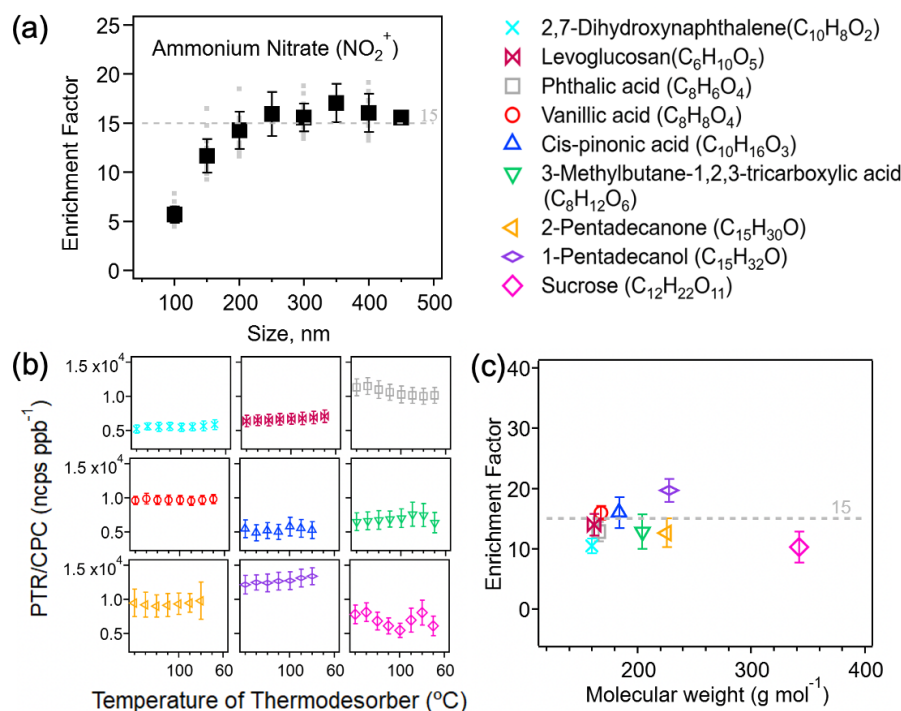


Figure 1. (a) Measured unitless enrichment factor (EF) of ammonium nitrate particles as a function of particle size in the 100–450 nm range. Grey markers represent all replicating measurements. The error bar denotes 1 standard deviation (1σ) of the average. (b) Ratios of PTR-ToF-MS signals (including both parent and fragment ions) to CPC counts ($\pm 1\sigma$) at 300 nm for all organic standards studied. (c) EF ($\pm 1\sigma$) of selected organic standards based on the calculated sensitivity.

ions) for each organic standard analyzed were stable within 15%, as shown in Fig. 1b. Also note that we did not observe any ions produced from decarboxylation and/or dehydration during the particle evaporation process. This is because the relative low operation temperature and the short heat exposure time could effectively limit any thermal dissociation of organic molecules. This demonstrates that the parent molecule fragmentation, if any, does not occur under the range of desorption temperature used in the CHARON inlet but rather results from the ionic dissociation process in the PTR ionization chamber; see more discussions in Sect. 3.3. We therefore used the sum total of intensities of all major ions detected as the PTR-ToF-MS response to a given organic standard analyzed. Figure 1c shows that the derived enrichment factors stay constant for all compounds investigated ($M_w \sim 160\text{--}230\text{ g mol}^{-1}$). The relative signals of all fragment ions were stable over the range of the desorption temperature as shown in Fig. 2. This suggests that the desorption temperature used here, even as low as 70°C , is sufficient to evaporate SVOCs (volatility $> 10^{-14}\text{ Pa}$ at 25°C), due to the low operating pressure ($\sim 8\text{ mbar}$) that significantly enhances the partitioning shift to the gas phase. One low-volatility compound, sucrose (M_w is 342 g mol^{-1} and vapor pressure is $4.69 \times 10^{-14}\text{ Pa}$), has a slightly lower enhancement factor compared with all the other organic standards tested. This is mainly due to the intensive dehydration

of the parent compound in the ionization chamber, and as a result, only a few fragment ions were captured, resulting in a lower PTR response and thereby lower EF value calculated from Eqs. (3)–(5). The EF values of sucrose also have much higher standard deviations at all temperatures due to fragmentation (Table S3).

It has been recognized that species with one functional group follow certain fragmentation patterns during the PTR ionization process (Pagonis et al., 2019; Francis et al., 2007; Spanel et al., 1997; Tani et al., 2003; Spanel and Smith, 1997), such as dehydration of acids and alcohols. The observed dissociation of carboxylic acid standards used in this study, e.g., phthalic acid and 3-methylbutane-1,2,3-tricarboxylic acid, can be explained by this common fragmentation pattern. The fragmentation mechanism of multifunctionalized species is rather complicated, and a number of fragments can be produced upon PTR ionization. Nevertheless, the identity and abundance of fragments from a given multifunctionalized species have been found comparable under the same PTR operation protocols (Leglise et al., 2019; Gkatzelis et al., 2018a). For example, *cis*-pinonic acid yields the following fragments (main ions only and relative abundance in parentheses): m/z 71.049 ($\sim 28\%$), 115.075 ($\sim 36\%$), 167.108 ($\sim 19\%$), and 185.117 ($\sim 11\%$), which are comparable with an earlier study (Leglise et al., 2019) with

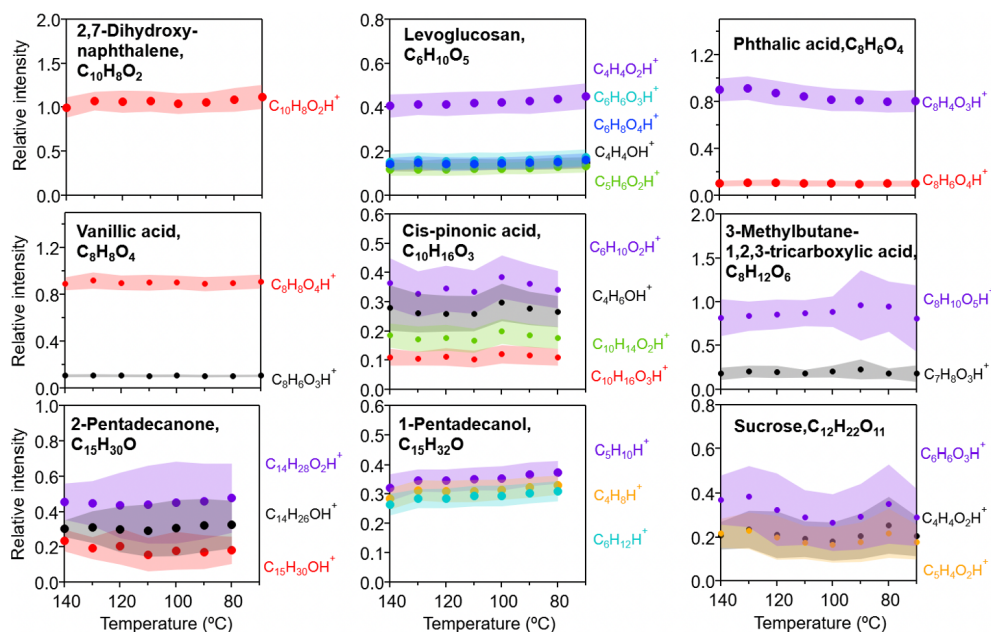


Figure 2. Ratios of CHARON-PTR-ToF-MS signals (ncps) to CPC measurements (ppb) of all detected ions (including both parents and fragments) for a given pure organic standard tested under different desorption temperatures (70–140 °C), normalized to the corresponding ratios obtained at 140 °C. Ions with relative intensities less than 10 % are excluded. Red markers represent the parent peaks. Colored shades represent the relative standard deviations at different temperatures (exact values are given in Table S4).

results of m/z 71.049 (~ 27 %), 115.075 (~ 33 %), 167.108 (~ 26 %), and 185.117 (~ 14 %) at 100 Td settings.

3.2 Molecular features of detected organic species

A month-long field dataset of particle- and gas-phase organic species was collected at hourly resolution using the CHARON-PTR-ToF-MS instrument. A comparison of PTR-ToF-MS measurements with other techniques available on site was performed for both gas and particle phases. For the gas phase, quantitative measurements of a suite of VOCs by GC-MS/FID, including benzene, toluene, styrene, C_8 and C_9 aromatics, acrolein, and C_4 , C_5 , and C_6 ketones, agree well with corresponding PTR-ToF-MS measurements, as shown in Fig. S6. For the particle phase, the time series of a group of $C_xH_yO_4$ species (including $C_4H_6O_4$, $C_5H_8O_4$, $C_6H_{10}O_4$, and $C_8H_6O_4$) are in reasonable agreement with corresponding measurements taken by TAG ($r \sim 0.60$ – 0.80), although the CHARON-PTR-ToF-MS-measured total molecular mass is generally lower than the TAG measurements by a factor of 2 to 6 (Fig. S7). This is likely caused by the fragmentation (e.g., loss of H_2O ; see Fig. S8) of the parent compounds during the ionization process, as discussed in detail in Sect. 3.3. The time series of total OA mass characterized by CHARON-PTR-ToF-MS also agree with the AMS measurements ($r \sim 0.91$, Fig. S9). Previous studies have reported the particulate organics measured by PTR-MS with a thermal desorption inlet account for 25 %–60 % mass of the total organic aerosols measured by AMS (Holzinger et al., 2013).

Direct comparison of the total OA mass loading is not applicable here since the CHARON-PTR-ToF-MS measurement only focused on compounds with a mass-to-charge ratio below 300 Th. That the majority of ions detected by PTR are present in the lower mass range is primarily due to the fragmentation of larger masses during the ionization process, as discussed extensively in Sect. 3.3.

Figure 3a–b show the PTR-ToF-MS spectra of dominant ions averaged over the entire campaign in both gas and particle phases. The mass concentrations of individual ions are in the range of 7.9–7179.3 $ng\ m^{-3}$ in the gas phase and 0.6–82.7 $ng\ m^{-3}$ in the particle phase. A total of 152 species (with > 60 % data points above the PTR-ToF-MS detection limits) are identified, contributing to ~ 69 % and ~ 44 %, respectively, of the total organic mass measured in the gas and particle phase. The molecular distribution characterized by the carbon and oxygen of these species is given in Fig. 3c–d. The most abundant species are characterized by a generic formula of C_xH_yO and $C_xH_yO_2$, resolving ~ 64 % and ~ 46 % in total of all identified species in the gas and particle phase, respectively. Another dominant component in the gas phase is hydrocarbon-like compounds (C_xH_y) (~ 27 %), which contribute ~ 12 % of the organic mass in the particle phase. Species with higher oxygen numbers (> 2) contribute to a large fraction (~ 42 %) of the total particulate mass. These $C_xH_yO_{1-4}$ groups exhibit different diurnal cycles, as shown in Fig. 4, reflecting their unique formation chemistry. The C_xH_y group peaks in the early morning rush hour and likely

originates from primary traffic emissions. On the contrary, both $C_xH_yO_3$ and $C_xH_yO_4$ groups peak at noon, suggesting a strong secondary formation source. The diurnal trends for C_xH_yO and $C_xH_yO_2$ groups are relatively flat during the day, likely indicative of an intertwined primary emission and secondary formation processes.

3.3 Measured vs. modeled gas–particle partitioning

Figure 5 shows the calculated particle-phase fraction (F_p) of the identified 152 species using the CHARON–PTR–ToF–MS measurements in both phases. It is important to note that an authentic standard is not required for the calculation of F_p for any given species because the PTR sensitivity term is essentially canceled in the divisor function in Eqs. (6)–(8). Also given in Fig. 5 is the simulated F_p of the derived molecular formulas of all species identified using equilibrium partitioning theory; see method described in Sect. 2.4. Interestingly, for oxidized species such as $C_xH_yO_4$, their measured F_p agree reasonably with the simulations, as shown in Fig. 5a. The $C_xH_yO_4$ group resides in the relatively higher mass range, and species identified in this group are more likely actual compounds rather than fragments from larger parent molecules. Even these species dissociate into lower-mass ions during PTR ionization; their calculated particle-phase fractions are unaffected by such fragmentation processes because signals of parent ions decrease by the same extent upon fragmentation in both gas and particle phases. As the oxygen number decreases, the measured F_p values tend to deviate from the simulations by up to several orders of magnitude. Note that these less oxidized compounds (e.g., C_xH_y) are mostly small molecules, and they are highly unlikely present in the condensed phase as closed-shell monomers (Pankow and Asher, 2008; Holzinger et al., 2010). Instead, they are more likely fragments produced from the decomposition of larger molecules, which not surprisingly favor partitioning in the particle phase. It is worth noting that the uptake of small oxidized compounds in the aerosol aqueous phase does not significantly affect the overall particle phase fraction of these compounds; see detailed calculations in Sect. S3. The discrepancy in the measurement–model comparison underscores the importance of understanding the fragmentation mechanism during PTR ionization when extracting molecular features from the raw mass spectra.

Parent ion fragmentation has been widely observed in PTR–MS instruments (Pagonis et al., 2019). Oxygenates exhibit trends in neutral losses of water or saturated alcohols. Here, we apply a correction to the molecular formula of the 152 identified species by assuming that these species are fragments produced from their parent precursors through the neutral losses of a carboxyl group ($-CO_2$), a carbonyl group ($-CO$), a hydroxyl group ($-H_2O$), or an alcohol group ($-C_2H_6O$). By applying this correction, the modeled F_p of a given species $C_xH_yO_z$ would actually represent the particle-phase fraction of the its parent species $C_xH_yO_z \bullet CO_2$,

$C_xH_yO_z \bullet CO$, $C_xH_yO_z \bullet H_2O$, or $C_xH_yO_z \bullet C_2H_6O$. As shown in Fig. 5b–e, such a correction could significantly increase the modeled F_p values by several orders of magnitude. The assumption of neutral losses of CO_2 or C_2H_6O allows for much improved agreement between modeled and measured F_p values for less oxidized species. This implies that these small and less oxidized species are likely fragments resulting from the decomposition of larger parent precursors. As our particle enrichment test (details given in Sect. 3.1) has confirmed that the thermal desorption temperature employed for particle evaporation does not lead to any intensive fragmentation, the collision-induced dissociation during the proton transfer reaction process becomes the predominant process that produces fragments (Lindinger et al., 1998; Gueneron et al., 2015; Gkatzelis et al., 2018b). Although the electric field applied to the drift tube is considered low to moderate compared with most previous PTR–MS measurements ($E/N \sim 100$ Td in this study vs. $E/N \sim 120$ – 140 Td commonly found in PTR–MS measurements) (Pagonis et al., 2019), parent ion fragmentation was still widely observed here and complicated the mass spectra interpretation and molecular feature extraction. While some recent CHARON measurements employed lower electric field in the drift tube ($E/N \sim 60$ Td) (Leglise et al., 2019; Gkatzelis et al., 2018a; Piel et al., 2019), such conditions could promote the formation of water cluster ions, which increase with humidity and reduce the PTR sensitivity and therefore are not ideally suitable for our field measurements. As a compromise, a solution would be to use a moderate electric field in the drift tube (e.g., ~ 100 Td) and meanwhile apply appropriate molecular corrections to all ions detected in the mass spectra by considering possible neutral losses of small moieties. Since in this study only the information of molecular formula is derived from the PTR–MS spectra, we provide the lower and upper bound of the gas–particle partitioning corrections owing to neutral losses of H_2O and CO_2 , respectively. In general, lower masses with higher volatilities are subject to notable changes in the particle-phase fraction as a result of neutral losses during the PTR ionization process; see detailed discussions in Sect. S2.

4 Conclusions

Recent studies have suggested that some of the model–measurement discrepancies in the representation of ambient organic aerosol budget might be due to the nonequilibrium gas–particle partitioning caused by kinetic limitations in the presence of particles that are glassy or semi-solid (Perraud et al., 2012; Mai et al., 2015; Shiraiwa et al., 2013). It is therefore necessary to validate whether equilibrium partitioning theory could adequately describe the condensation of semivolatile organic vapors onto atmospheric aerosols under ambient conditions, and the accurate measurement of these SVOCs in both gas and particle phases is the crucial

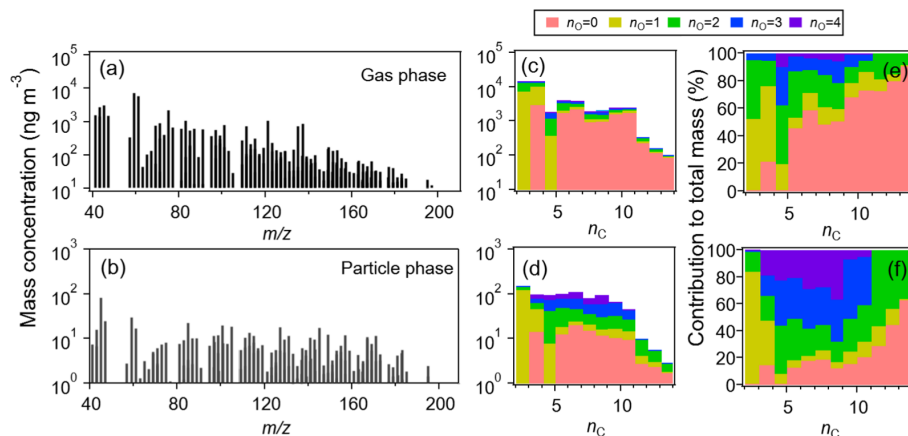


Figure 3. Background subtracted monthly-average PTR-ToF-MS mass spectra in the (a) gas phase and (b) particle phase. Mass distributions of all identified species resolved by the carbon and oxygen numbers (n_C and n_O) in the (c) gas phase and (d) particle phase, as well as their relative contribution to the total organic mass in the (e) gas phase and (f) particle phase.

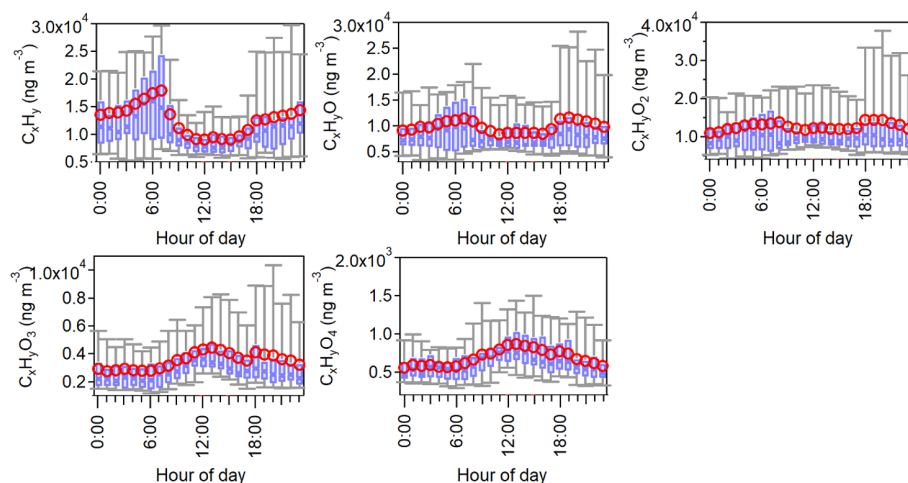


Figure 4. Diurnal variations of observed gas-phase species with a generic formula of $C_{2-13}H_{2-22}O_{0-4}$. Hourly average values (ng m^{-3}), together with 10th, 25th, 75th, and 90th percentiles, are also plotted.

prerequisite. In this study, we have employed the PTR-ToF-MS instrument coupled to a CHARON inlet, together with a suite of complementary measurements, to characterize the atmospheric partitioning behaviors of an array of SVOCs in an urban environment of East China. Prior to the application to the field measurements, we first performed a series of laboratory experiments to test whether the CHARON inlet is capable of sampling organic molecules (including alcohols, carbonyls, and carboxylic acids) in their native states. With the low-pressure condition used in the CHARON inlet, a thermal desorption temperature less than 140°C could adequately evaporate organic compounds with vapor pressure higher than 10^{-14} Pa while minimizing the thermal decomposition of labile functionalities. The auto-switch function between the gas and particle mode with one single PTR-ToF-MS instrument could monitor gaseous and particulate organic compounds in real time, thereby providing impor-

tant information of their partitioning behaviors in the ambient atmosphere. Particle-phase fractions of a total of 152 organic species were derived from the CHARON-PTR-ToF-MS measurements and further compared with model predictions using instantaneous equilibrium partitioning theory. While the model captured the particle-phase fraction of oxidized compounds (e.g., $C_xH_yO_{3-4}$), predictions of less oxidized compounds, notably the C_xH_y family, differ from the corresponding measurements by several orders of magnitude. Such a large discrepancy is very likely caused by the intensive fragmentation of the parent organic compounds during the PTR ionization process. Accounting for common fragmentation patterns in the simulations of gas-particle partitioning, for example, neutral losses of $-\text{CO}_2$, $-\text{CO}$, $-\text{H}_2\text{O}$, or $-\text{C}_2\text{H}_6\text{O}$, could largely improve the model-measurement agreement. Such corrections are very necessary towards an accurate measurement of both particle- and

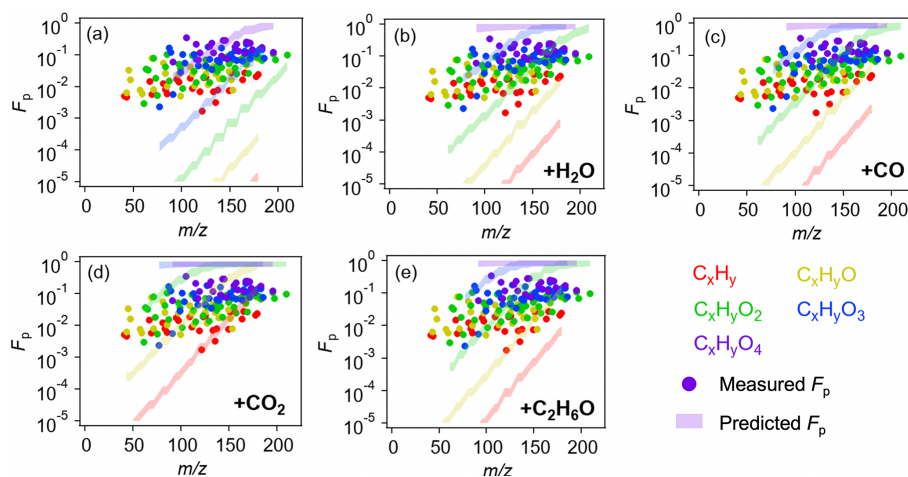


Figure 5. (a) Campaign average fraction of organic species in the particle phase (F_p) grouped by oxygen number. Solid markers represent the calculated F_p based on the CHARON-PTR-ToF-MS measurements. Colored shading represents the predicted F_p of corresponding molecular formulas. (b–e) Measured vs. predicted F_p , assuming the identified species are fragments of corresponding parent compounds through neutral losses of H_2O , CO , CO_2 , and C_2H_6O , respectively (values are given in Table S5).

gas-phase SVOCs using the CHARON-PTR-ToF-MS instrument. Our study suggests the crucial importance of optimizing operation conditions and understanding the fragmentation mechanism in the particle collection, vaporization, and ionization processes in understanding the gas–particle partitioning of organic compounds using any thermal-desorption-based aerosol measurement method.

Data availability. The data shown in the paper are available upon request from the corresponding author.

Supplement. The supplement related to this article is available online at: <https://doi.org/10.5194/amt-16-15-2023-supplement>.

Author contributions. YP carried out experiments and measurements and drafted the manuscript. HW and XZ designed the experimental studies, supervised the laboratory work, and wrote the manuscript. YG and SJ supported the ambient measurements. SZ, DH, PH, and SL supported the data analysis. TC and CH supervised the scientific work. All authors have given approval to the final version of the manuscript.

Competing interests. The contact author has declared that none of the authors has any competing interests.

Disclaimer. Publisher’s note: Copernicus Publications remains neutral with regard to jurisdictional claims in published maps and institutional affiliations.

Acknowledgements. This research has been supported by the National Natural Science Foundation of China (grant nos. 42175135 and 42175179), the National Key R&D Program of China (grant no. 2022YFE0136200), and the Shanghai Science and Technology Commission of the Shanghai Municipality (grant no. 20ZR1447800).

Financial support. This research has been supported by the National Natural Science Foundation of China (grant nos. 42175135 and 42175179) and the Science and Technology Commission of Shanghai Municipality (grant no. 20ZR1447800) and the National Key R&D Program of China (grant no. 2022YFE0136200).

Review statement. This paper was edited by Mingjin Tang and reviewed by two anonymous referees.

References

- Antonsen, S., Bunkan, A. J. C., D’Anna, B., Eichler, P., Farren, N., Hallquist, M., Hamilton, J. F., Kvarnliden, H., Mikoviny, T., Muller, M., Nielsen, C. J., Stenstrom, Y., Tan, W., Wisthaler, A., and Zhu, L.: Atmospheric chemistry of tert-butylamine and AMP, in: *Energy Procedia*, edited by: Dixon, T., Laloui, L., and Twinning, S., *Energy Procedia*, Elsevier Science Bv, Amsterdam, 1026–1032, doi:10.1016/j.egypro.2017.03.1248, 2017.
- Crouse, J. D., McKinney, K. A., Kwan, A. J., and Wennberg, P. O.: Measurement of gas-phase hydroperoxides by chemical ionization mass spectrometry, *Anal. Chem.*, 78, 6726–6732, <https://doi.org/10.1021/ac0604235>, 2006.
- de Gouw, J. and Warneke, C.: Measurements of volatile organic compounds in the earths atmosphere using proton-transfer-reaction mass spectrometry, *Mass Spectrom. Rev.*, 26, 223–257, <https://doi.org/10.1002/mas.20119>, 2007.

- Donahue, N. M., Epstein, S. A., Pandis, S. N., and Robinson, A. L.: A two-dimensional volatility basis set: 1. organic-aerosol mixing thermodynamics, *Atmos. Chem. Phys.*, 11, 3303–3318, <https://doi.org/10.5194/acp-11-3303-2011>, 2011.
- Eichler, P., Müller, M., D'Anna, B., and Wisthaler, A.: A novel inlet system for online chemical analysis of semi-volatile sub-micron particulate matter, *Atmos. Meas. Tech.*, 8, 1353–1360, <https://doi.org/10.5194/amt-8-1353-2015>, 2015.
- Eichler, P., Müller, M., Rohmann, C., Stengel, B., Orasche, J., Zimmermann, R., and Wisthaler, A.: Lubricating Oil as a Major Constituent of Ship Exhaust Particles, *Environ. Sci. Technol. Lett.*, 4, 54–58, <https://doi.org/10.1021/acs.estlett.6b00488>, 2017.
- EPA: Estimation Programs Interface (EPI) Suite for Microsoft Windows, v 4.11, United States Environmental Protection Agency, Washington, DC, USA, 2012.
- Francis, G. J., Milligan, D. B., and McEwan, M. J.: Gas-Phase Reactions and Rearrangements of Alkyl Esters with H_3O^+ , NO^+ , and O_2^+ : A Selected Ion Flow Tube Study, *J. Phys. Chem. A*, 111, 9670–9679, <https://doi.org/10.1021/jp0731304>, 2007.
- Gkatzelis, G. I., Tillmann, R., Hohaus, T., Müller, M., Eichler, P., Xu, K.-M., Schlag, P., Schmitt, S. H., Wegener, R., Kaminski, M., Holzinger, R., Wisthaler, A., and Kiendler-Scharr, A.: Comparison of three aerosol chemical characterization techniques utilizing PTR-ToF-MS: a study on freshly formed and aged biogenic SOA, *Atmos. Meas. Tech.*, 11, 1481–1500, <https://doi.org/10.5194/amt-11-1481-2018>, 2018a.
- Gkatzelis, G. I., Hohaus, T., Tillmann, R., Gensch, I., Müller, M., Eichler, P., Xu, K.-M., Schlag, P., Schmitt, S. H., Yu, Z., Wegener, R., Kaminski, M., Holzinger, R., Wisthaler, A., and Kiendler-Scharr, A.: Gas-to-particle partitioning of major biogenic oxidation products: a study on freshly formed and aged biogenic SOA, *Atmos. Chem. Phys.*, 18, 12969–12989, <https://doi.org/10.5194/acp-18-12969-2018>, 2018b.
- Gueneron, M., Erickson, M. H., VanderSchelden, G. S., and Jobson, B. T.: PTR-MS fragmentation patterns of gasoline hydrocarbons, *International J. Mass Spectrom.*, 379, 97–109, <https://doi.org/10.1016/j.ijms.2015.01.001>, 2015.
- He, X., Wang, Q., Huang, X. H. H., Huang, D. D., Zhou, M., Qiao, L., Zhu, S., Ma, Y.-g., Wang, H.-l., Li, L., Huang, C., Xu, W., Worsnop, D. R., Goldstein, A. H., and Yu, J. Z.: Hourly measurements of organic molecular markers in urban Shanghai, China: Observation of enhanced formation of secondary organic aerosol during particulate matter episodic periods, *Atmos. Environ.*, 240, 117807, <https://doi.org/10.1016/j.atmosenv.2020.117807>, 2020.
- Heald, C. L. and Kroll, J. H.: The fuel of atmospheric chemistry: Toward a complete description of reactive organic carbon, *Sci. Adv.*, 6, eaay8967, <https://doi.org/10.1126/sciadv.aay8967>, 2020.
- Holzinger, R., Goldstein, A. H., Hayes, P. L., Jimenez, J. L., and Timkovsky, J.: Chemical evolution of organic aerosol in Los Angeles during the CalNex 2010 study, *Atmos. Chem. Phys.*, 13, 10125–10141, <https://doi.org/10.5194/acp-13-10125-2013>, 2013.
- Holzinger, R., Williams, J., Herrmann, F., Lelieveld, J., Donahue, N. M., and Röckmann, T.: Aerosol analysis using a Thermal-Desorption Proton-Transfer-Reaction Mass Spectrometer (TD-PTR-MS): a new approach to study processing of organic aerosols, *Atmos. Chem. Phys.*, 10, 2257–2267, <https://doi.org/10.5194/acp-10-2257-2010>, 2010.
- Holzinger, R., Acton, W. J. F., Bloss, W. J., Breitenlechner, M., Crilley, L. R., Dusanter, S., Gonin, M., Gros, V., Keutsch, F. N., Kiendler-Scharr, A., Kramer, L. J., Krechmer, J. E., Languille, B., Locoge, N., Lopez-Hilfiker, F., Materić, D., Moreno, S., Nemitz, E., Quéléver, L. L. J., Sarda Esteve, R., Sauvage, S., Schallhart, S., Sommariva, R., Tillmann, R., Wedel, S., Worton, D. R., Xu, K., and Zaytsev, A.: Validity and limitations of simple reaction kinetics to calculate concentrations of organic compounds from ion counts in PTR-MS, *Atmos. Meas. Tech.*, 12, 6193–6208, <https://doi.org/10.5194/amt-12-6193-2019>, 2019.
- Huang, D. D., Zhu, S., An, J., Wang, Q., Qiao, L., Zhou, M., He, X., Ma, Y., Sun, Y., Huang, C., Yu, J. Z., and Zhang, Q.: Comparative Assessment of Cooking Emission Contributions to Urban Organic Aerosol Using Online Molecular Tracers and Aerosol Mass Spectrometry Measurements, *Environ. Sci. Technol.*, 55, 14526–14535, <https://doi.org/10.1021/acs.est.1c03280>, 2021.
- Huang, G., Liu, Y., Shao, M., Li, Y., Chen, Q., Zheng, Y., Wu, Z., Liu, Y., Wu, Y., Hu, M., Li, X., Lu, S., Wang, C., Liu, J., Zheng, M., and Zhu, T.: Potentially Important Contribution of Gas-Phase Oxidation of Naphthalene and Methyl-naphthalene to Secondary Organic Aerosol during Haze Events in Beijing, *Environ. Sci. Technol.*, 53, 1235–1244, <https://doi.org/10.1021/acs.est.8b04523>, 2019.
- Inomata, S., Sato, K., Hirokawa, J., Sakamoto, Y., Tanimoto, H., Okumura, M., Tohno, S., and Imamura, T.: Analysis of secondary organic aerosols from ozonolysis of isoprene by proton transfer reaction mass spectrometry, *Atmos. Environ.*, 97, 397–405, <https://doi.org/10.1016/j.atmosenv.2014.03.045>, 2014.
- Krechmer, J. E., Groessl, M., Zhang, X., Junninen, H., Massoli, P., Lambe, A. T., Kimmel, J. R., Cubison, M. J., Graf, S., Lin, Y.-H., Budisulistiorini, S. H., Zhang, H., Surratt, J. D., Knochenmuss, R., Jayne, J. T., Worsnop, D. R., Jimenez, J.-L., and Canagaratna, M. R.: Ion mobility spectrometry–mass spectrometry (IMS–MS) for on- and offline analysis of atmospheric gas and aerosol species, *Atmos. Meas. Tech.*, 9, 3245–3262, <https://doi.org/10.5194/amt-9-3245-2016>, 2016.
- Le Breton, M., Wang, Y., Hallquist, Å. M., Pathak, R. K., Zheng, J., Yang, Y., Shang, D., Glasius, M., Bannan, T. J., Liu, Q., Chan, C. K., Percival, C. J., Zhu, W., Lou, S., Topping, D., Wang, Y., Yu, J., Lu, K., Guo, S., Hu, M., and Hallquist, M.: Online gas- and particle-phase measurements of organosulfates, organosulfonates and nitrooxy organosulfates in Beijing utilizing a FI-GAERO ToF-CIMS, *Atmos. Chem. Phys.*, 18, 10355–10371, <https://doi.org/10.5194/acp-18-10355-2018>, 2018.
- Lee, B. H., Lopez-Hilfiker, F. D., D'Ambro, E. L., Zhou, P., Boy, M., Petäjä, T., Hao, L., Virtanen, A., and Thornton, J. A.: Semi-volatile and highly oxygenated gaseous and particulate organic compounds observed above a boreal forest canopy, *Atmos. Chem. Phys.*, 18, 11547–11562, <https://doi.org/10.5194/acp-18-11547-2018>, 2018.
- Leglise, J., Müller, M., Piel, F., Otto, T., and Wisthaler, A.: Bulk Organic Aerosol Analysis by Proton-Transfer-Reaction Mass Spectrometry: An Improved Methodology for the Determination of Total Organic Mass, O:C and H:C Elemental Ratios, and the Average Molecular Formula, *Anal. Chem.*, 91, 12619–12624, <https://doi.org/10.1021/acs.analchem.9b02949>, 2019.
- Lindinger, W., Hansel, A., and Jordan, A.: Proton-transfer-reaction mass spectrometry (PTR-MS): on-line monitoring of volatile or-

- ganic compounds at pptv levels, *Chem. Soc. Rev.*, 27, 347–354, <https://doi.org/10.1039/a827347z>, 1998.
- Lopez-Hilfiker, F. D., Mohr, C., Ehn, M., Rubach, F., Kleist, E., Wildt, J., Mentel, Th. F., Lutz, A., Hallquist, M., Worsnop, D., and Thornton, J. A.: A novel method for online analysis of gas and particle composition: description and evaluation of a Filter Inlet for Gases and AEROSols (FIGAERO), *Atmos. Meas. Tech.*, 7, 983–1001, <https://doi.org/10.5194/amt-7-983-2014>, 2014.
- Lopez-Hilfiker, F. D., Mohr, C., Ehn, M., Rubach, F., Kleist, E., Wildt, J., Mentel, Th. F., Carrasquillo, A. J., Daumit, K. E., Hunter, J. F., Kroll, J. H., Worsnop, D. R., and Thornton, J. A.: Phase partitioning and volatility of secondary organic aerosol components formed from α -pinene ozonolysis and OH oxidation: the importance of accretion products and other low volatility compounds, *Atmos. Chem. Phys.*, 15, 7765–7776, <https://doi.org/10.5194/acp-15-7765-2015>, 2015.
- Lopez-Hilfiker, F. D., Mohr, C., D'Ambro, E. L., Lutz, A., Riedel, T. P., Gaston, C. J., Iyer, S., Zhang, Z., Gold, A., Surratt, J. D., Lee, B. H., Kurten, T., Hu, W. W., Jimenez, J., Hallquist, M., and Thornton, J. A.: Molecular Composition and Volatility of Organic Aerosol in the Southeastern U.S.: Implications for IEPOX Derived SOA, *Environ. Sci. Technol.*, 50, 2200–2209, <https://doi.org/10.1021/acs.est.5b04769>, 2016.
- Lutz, A., Mohr, C., Le Breton, M., Lopez-Hilfiker, F. D., Priestley, M., Thornton, J. A., and Hallquist, M.: Gas to Particle Partitioning of Organic Acids in the Boreal Atmosphere, *ACS Earth Space Chem.*, 3, 1279–1287, <https://doi.org/10.1021/acsearthspacechem.9b00041>, 2019.
- Mai, H., Shiraiwa, M., Flagan, R. C., and Seinfeld, J. H.: Under What Conditions Can Equilibrium Gas-Particle Partitioning Be Expected to Hold in the Atmosphere?, *Environ. Sci. Technol.*, 49, 11485–11491, <https://doi.org/10.1021/acs.est.5b02587>, 2015.
- Muller, M., Eichler, P., D'Anna, B., Tan, W., and Wisthaler, A.: Direct Sampling and Analysis of Atmospheric Particulate Organic Matter by Proton-Transfer-Reaction Mass Spectrometry, *Anal. Chem.*, 89, 10889–10897, <https://doi.org/10.1021/acs.analchem.7b02582>, 2017.
- Pagonis, D., Sekimoto, K., and de Gouw, J.: A Library of Proton-Transfer Reactions of H₃O⁺ Ions Used for Trace Gas Detection, *J. Am. Soc. Mass Spectrom.*, 30, 1330–1335, <https://doi.org/10.1007/s13361-019-02209-3>, 2019.
- Palm, B. B., Peng, Q. Y., Fredrickson, C. D., Lee, B., Garofalo, L. A., Pothier, M. A., Kreidenweis, S. M., Farmer, D. K., Pokhrel, R. P., Shen, Y. J., Murphy, S. M., Permar, W., Hu, L., Campos, T. L., Hall, S. R., Ullmann, K., Zhang, X., Flocke, F., Fischer, E. V., and Thornton, J. A.: Quantification of organic aerosol and brown carbon evolution in fresh wildfire plumes, *P. Natl. Acad. Sci. USA*, 117, 29469–29477, <https://doi.org/10.1073/pnas.2012218117>, 2020.
- Pankow, J. F.: An absorption-model of the gas aerosol partitioning involved in the formation of secondary organic aerosol, *Atmos. Environ.*, 28, 189–193, [https://doi.org/10.1016/1352-2310\(94\)90094-9](https://doi.org/10.1016/1352-2310(94)90094-9), 1994.
- Pankow, J. F. and Asher, W. E.: SIMPOL.1: a simple group contribution method for predicting vapor pressures and enthalpies of vaporization of multifunctional organic compounds, *Atmos. Chem. Phys.*, 8, 2773–2796, <https://doi.org/10.5194/acp-8-2773-2008>, 2008.
- Peng, Y., Wang, H., Wang, Q., Jing, S., An, J., Gao, Y., Huang, C., Yan, R., Dai, H., Cheng, T., Zhang, Q., Li, M., Hu, J., Shi, Z., Li, L., Lou, S., Tao, S., Hu, Q., Lu, J., and Chen, C.: Observation-based sources evolution of non-methane hydrocarbons (NMHCs) in a megacity of China, *J. Environ. Sci.*, 124, 794–805, <https://doi.org/10.1016/j.jes.2022.01.040>, 2023.
- Perraud, V., Bruns, E. A., Ezell, M. J., Johnson, S. N., Yu, Y., Alexander, M. L., Zelenyuk, A., Imre, D., Chang, W. L., Dabdub, D., Pankow, J. F., and Finlayson-Pitts, B. J.: Nonequilibrium atmospheric secondary organic aerosol formation and growth, *P. Natl. Acad. Sci. USA*, 109, 2836–2841, <https://doi.org/10.1073/pnas.1119909109>, 2012.
- Piel, F., Müller, M., Mikoviny, T., Pusede, S. E., and Wisthaler, A.: Airborne measurements of particulate organic matter by proton-transfer-reaction mass spectrometry (PTR-MS): a pilot study, *Atmos. Meas. Tech.*, 12, 5947–5958, <https://doi.org/10.5194/amt-12-5947-2019>, 2019.
- Piel, F., Müller, M., Winkler, K., Skytte af Sättra, J., and Wisthaler, A.: Introducing the extended volatility range proton-transfer-reaction mass spectrometer (EVR PTR-MS), *Atmos. Meas. Tech.*, 14, 1355–1363, <https://doi.org/10.5194/amt-14-1355-2021>, 2021.
- Sekimoto, K., Li, S. M., Yuan, B., Koss, A., Coggon, M., Warneke, C., and de Gouw, J.: Calculation of the sensitivity of proton-transfer-reaction mass spectrometry (PTR-MS) for organic trace gases using molecular properties, *Int. J. Mass Spectrom.*, 421, 71–94, <https://doi.org/10.1016/j.ijms.2017.04.006>, 2017.
- Shiraiwa, M. and Seinfeld, J. H.: Equilibration timescale of atmospheric secondary organic aerosol partitioning, *Geophys. Res. Lett.*, 39, L24801, <https://doi.org/10.1029/2012gl054008>, 2012.
- Shiraiwa, M., Zuend, A., Bertram, A. K., and Seinfeld, J. H.: Gas-particle partitioning of atmospheric aerosols: interplay of physical state, non-ideal mixing and morphology, *Phys. Chem. Chem. Phys.*, 15, 11441–11453, <https://doi.org/10.1039/c3cp51595h>, 2013.
- Spanel, P. and Smith, D.: SIFT studies of the reactions of H₃O⁺, NO⁺ and O₂⁺ with a series of alcohols, *Int. J. Mass Spectrom. Ion Processes*, 167–168, 375–388, [https://doi.org/10.1016/S0168-1176\(97\)00085-2](https://doi.org/10.1016/S0168-1176(97)00085-2), 1997.
- Spanel, P., Ji, Y. F., and Smith, D.: SIFT studies of the reactions of H₃O⁺, NO⁺ and O₂⁺ with a series of aldehydes and ketones, *Int. J. Mass Spectrom.*, 165, 25–37, [https://doi.org/10.1016/s0168-1176\(97\)00166-3](https://doi.org/10.1016/s0168-1176(97)00166-3), 1997.
- Stark, H., Yatavelli, R. L. N., Thompson, S. L., Kang, H., Krechmer, J. E., Kimmel, J. R., Palm, B. B., Hu, W. W., Hayes, P. L., Day, D. A., Campuzano-Jost, P., Canagaratna, M. R., Jayne, J. T., Worsnop, D. R., and Jimenez, J. L.: Impact of Thermal Decomposition on Thermal Desorption Instruments: Advantage of Thermogram Analysis for Quantifying Volatility Distributions of Organic Species, *Environ. Sci. Technol.*, 51, 8491–8500, <https://doi.org/10.1021/acs.est.7b00160>, 2017.
- Tan, W., Zhu, L., Mikoviny, T., Nielsen, C. J., Wisthaler, A., Eichler, P., Muller, M., D'Anna, B., Farren, N. J., Hamilton, J. F., Pettersson, J. B. C., Hallquist, M., Antonsen, S., and Stenstrom, Y.: Theoretical and Experimental Study on the Reaction of tert-Butylamine with OH Radicals in the Atmosphere, *J. Phys. Chem. A*, 122, 4470–4480, <https://doi.org/10.1021/acs.jpca.8b01862>, 2018.

- Tani, A., Hayward, S., and Hewitta, C. N.: Measurement of monoterpenes and related compounds by proton transfer reaction-mass spectrometry (PTR-MS), *Int. J. Mass Spectrom.*, 223, 561–578, [https://doi.org/10.1016/s1387-3806\(02\)00880-1](https://doi.org/10.1016/s1387-3806(02)00880-1), 2003.
- Thompson, S. L., Yatavelli, R. L. N., Stark, H., Kimmel, J. R., Krechmer, J. E., Day, D. A., Hu, W., Isaacman-VanWertz, G., Yee, L., Goldstein, A. H., Khan, M. A. H., Holzinger, R., Kreisberg, N., Lopez-Hilfiker, F. D., Mohr, C., Thornton, J. A., Jayne, J. T., Canagaratna, M., Worsnop, D. R., and Jimenez, J. L.: Field intercomparison of the gas/particle partitioning of oxygenated organics during the Southern Oxidant and Aerosol Study (SOAS) in 2013, *Aerosol Sci. Technol.*, 51, 30–56, <https://doi.org/10.1080/02786826.2016.1254719>, 2016.
- Veres, P., Roberts, J. M., Warneke, C., Welsh-Bon, D., Zahniser, M., Herndon, S., Fall, R., and de Gouw, J.: Development of negative-ion proton-transfer chemical-ionization mass spectrometry (NI-PT-CIMS) for the measurement of gas-phase organic acids in the atmosphere, *Int. J. Mass Spectrom.*, 274, 48–55, <https://doi.org/10.1016/j.ijms.2008.04.032>, 2008.
- Voliotis, A., Wang, Y., Shao, Y., Du, M., Bannan, T. J., Percival, C. J., Pandis, S. N., Alfara, M. R., and McFiggans, G.: Exploring the composition and volatility of secondary organic aerosols in mixed anthropogenic and biogenic precursor systems, *Atmos. Chem. Phys.*, 21, 14251–14273, <https://doi.org/10.5194/acp-21-14251-2021>, 2021.
- Wang, H. L., Lou, S. R., Huang, C., Qiao, L. P., Tang, X. B., Chen, C. H., Zeng, L. M., Wang, Q., Zhou, M., Lu, S. H., and Yu, X. N.: Source Profiles of Volatile Organic Compounds from Biomass Burning in Yangtze River Delta, China, *Aerosol Air Qual. Res.*, 14, 818–828, <https://doi.org/10.4209/aaqr.2013.05.0174>, 2014.
- Wang, M. Y., Chen, D. X., Xiao, M., Ye, Q., Stolzenburg, D., Hofbauer, V., Ye, P. L., Vogel, A. L., Mauldin, R. L., Amorim, A., Baccarini, A., Baumgartner, B., Brilke, S., Dada, L., Dias, A., Duplissy, J., Finkenzeller, H., Garmash, O., He, X. C., Hoyle, C. R., Kim, C., Kvashnin, A., Lehtipalo, K., Fischer, L., Molteni, U., Petaja, T., Pospisilova, V., Quelever, L. L. J., Rissanen, M., Simon, M., Tauber, C., Tome, A., Wagner, A. C., Weitz, L., Volkamer, R., Winkler, P. M., Kirkby, J., Worsnop, D. R., Kulmala, M., Baltensperger, U., Dommen, J., El Haddad, I., and Donahue, N. M.: Photo-oxidation of Aromatic Hydrocarbons Produces Low-Volatility Organic Compounds, *Environ. Sci. Technol.*, 54, 7911–7921, 2020a.
- Wang, Q. Q., He, X., Zhou, M., Huang, D. D., Qiao, L. P., Zhu, S. H., Ma, Y. G., Wang, H. L., Li, L., Huang, C., Huang, X. H. H., Xu, W., Worsnop, D., Goldstein, A. H., Guo, H., and Yu, J. Z.: Hourly Measurements of Organic Molecular Markers in Urban Shanghai, China: Primary Organic Aerosol Source Identification and Observation of Cooking Aerosol Aging, *ACS Earth Space Chem.*, 4, 1670–1685, 2020b.
- Yatavelli, R. L. N., Lopez-Hilfiker, F., Wargo, J. D., Kimmel, J. R., Cubison, M. J., Bertram, T. H., Jimenez, J. L., Gonin, M., Worsnop, D. R., and Thornton, J. A.: A Chemical Ionization High-Resolution Time-of-Flight Mass Spectrometer Coupled to a Micro Orifice Volatilization Impactor (MOVI-HRToF-CIMS) for Analysis of Gas and Particle-Phase Organic Species, *Aerosol Sci. Technol.*, 46, 1313–1327, 2012.
- Ye, C., Yuan, B., Lin, Y., Wang, Z., Hu, W., Li, T., Chen, W., Wu, C., Wang, C., Huang, S., Qi, J., Wang, B., Wang, C., Song, W., Wang, X., Zheng, E., Krechmer, J. E., Ye, P., Zhang, Z., Wang, X., Worsnop, D. R., and Shao, M.: Chemical characterization of oxygenated organic compounds in the gas phase and particle phase using iodide CIMS with FIGAERO in urban air, *Atmos. Chem. Phys.*, 21, 8455–8478, <https://doi.org/10.5194/acp-21-8455-2021>, 2021.
- Zhang, X. and Seinfeld, J. H.: A functional group oxidation model (FGOM) for SOA formation and aging, *Atmos. Chem. Phys.*, 13, 5907–5926, <https://doi.org/10.5194/acp-13-5907-2013>, 2013.
- Zhang, X., Dalleska, N. F., Huang, D. D., Bates, K. H., Sorooshian, A., Flagan, R. C., and Seinfeld, J. H.: Time-resolved molecular characterization of organic aerosols by PILS plus UPLC/ESI-Q-TOFMS, *Atmos. Environ.*, 130, 180–189, <https://doi.org/10.1016/j.atmosenv.2015.08.049>, 2016a.
- Zhang, X., Zhang, H., Xu, W., Wu, X., Tyndall, G. S., Orlando, J. J., Jayne, J. T., Worsnop, D. R., and Canagaratna, M. R.: Molecular characterization of alkyl nitrates in atmospheric aerosols by ion mobility mass spectrometry, *Atmos. Meas. Tech.*, 12, 5535–5545, <https://doi.org/10.5194/amt-12-5535-2019>, 2019.
- Zhang, X., Krechmer, J. E., Groessl, M., Xu, W., Graf, S., Cubison, M., Jayne, J. T., Jimenez, J. L., Worsnop, D. R., and Canagaratna, M. R.: A novel framework for molecular characterization of atmospherically relevant organic compounds based on collision cross section and mass-to-charge ratio, *Atmos. Chem. Phys.*, 16, 12945–12959, <https://doi.org/10.5194/acp-16-12945-2016>, 2016b.
- Zhao, Y. L., Kreisberg, N. M., Worton, D. R., Isaacman, G., Weber, R. J., Liu, S., Day, D. A., Russell, L. M., Markovic, M. Z., VandenBoer, T. C., Murphy, J. G., Hering, S. V., and Goldstein, A. H.: Insights into Secondary Organic Aerosol Formation Mechanisms from Measured Gas/Particle Partitioning of Specific Organic Tracer Compounds, *Environ. Sci. Technol.*, 47, 3781–3787, 2013.
- Zhu, H., Wang, H., Jing, S., Wang, Y., Cheng, T., Tao, S., Lou, S., Qiao, L., Li, L., and Chen, J.: Characteristics and sources of atmospheric volatile organic compounds (VOCs) along the mid-lower Yangtze River in China, *Atmos. Environ.*, 190, 232–240, <https://doi.org/10.1016/j.atmosenv.2018.07.026>, 2018.
- Zhu, S., Wang, Q., Qiao, L., Zhou, M., Wang, S., Lou, S., Huang, D., Wang, Q., Jing, S., Wang, H., Chen, C., Huang, C., and Yu, J. Z.: Tracer-based characterization of source variations of PM_{2.5} and organic carbon in Shanghai influenced by the COVID-19 lockdown, *Faraday Discuss.*, 226, 112–137, <https://doi.org/10.1039/d0fd00091d>, 2021.